# Experimental Results of a Quadrotor UAV with a Model Reference Adaptive Controller in the Presence of Unmodeled Dynamics

Stefan Ristevski*
*Combine Control Systems AB*

Ahmet Taha Koru†
*University of Texas at Arlington*

Tansel Yucelen‡
*University of South Florida*

K. Merve Dogan§
*Embry-Riddle Aeronautical University*

Jonathan A. Muse¶
*Air Force Research Laboratory*

**This paper presents experimental results related to the trajectory tracking performance of a recently developed model reference adaptive control (MRAC) of a quadrotor unmanned aerial vehicle carrying a suspended load under wind turbulance. The suspended load as an unmodeled dynamics and the wind as a constant disturbance significantly degrade the tracking performance of the nominal controller. We compare the performance of the mentioned MRAC with the performances of the nominal controller and the standard MRAC through a series of experiments to elucidate its efficacy in reducing the effects of unmodeled dynamics.**

## I Introduction

Addressing the presence of unmodeled dynamics, which stems from the interaction between rigid body dynamics and flexible appendages, is challenging for model reference adaptive control algorithms (we refer to introduction sections of [1,2] for related literature). In particular, the authors of [1] first show a sufficient

*Stefan Ristevski is Controls Engineer at Combine Controls Systems AB ( http://www.combine.se) Lund 41755, Sweden (email: stefan.ristevski@combine.se).

†Ahmet Taha Koru is a Postdoctoral Research Associate at the University of Texas at Arlington Research Institute, Fort Worth, TX 76118, USA (email: ahtakoru@gmail.com).

‡T. Yucelen is an Associate Professor of the Department of Mechanical Engineering and the Director of the Laboratory for Autonomy, Control, Information, and Systems (LACIS, http://lacis.eng.usf.edu/) at the University of South Florida, Tampa, FL 33620, USA (email: yucelen@usf.edu). T. Yucelen is also a Senior Member of the American Institute of Aeronautics and Astronautics and a Member of the National Academy of Inventors.

§K. Merve Dogan is an Assistant Professor of the Aerospace Engineering Department at the Embry-Riddle Aeronautical University, Daytona, FL 32114. USA (email: dogank@erau.edu).

¶J. A. Muse is a Research Aerospace Engineer of the Autonomous Control Branch at the Air Force Research Laboratory Aerospace Systems Directorate, WPAFB, Ohio 45433, USA (email: jonathan.muse.2@us.af.mil).

*This research was supported by the Air Force Research Laboratory Aerospace Systems Directorate under the Universal Technology Corporation Grant 17-S8401-02-C1.

Figure 1: Experimental scenario: Carrying a load while trajectory tracking. The colors of the photo is edited to highlight the rope and the load.

stability condition predicated on a projection operator that allows model reference adaptive control algorithms to work safely in the presence of unmodeled dynamics without constraining the uncertain dynamical system to start from a set of initial conditions and without requiring the persistency of excitation condition (see also [3–6] for other related work).

The authors of [Section 2, 2] also present a reinterpretation of this result with a similar conclusion that the model reference adaptive control algorithms remain stable either if there does not exist significant unmodeled dynamics or the effect of system uncertainties is negligible. To allow for these algorithms to remain stable in the presence of large system uncertainties when the unmodeled dynamics satisfy a set of conditions, [Section 3, 2] then present an adaptive robustifying term augmented with a standard model reference adaptive control algorithm predicated on projection operator, where a relaxed version of the mentioned sufficient stability condition is given (see also [7–11] for other related work).

This paper presents experimental results of the model reference adaptive control architecture in [Section 3, 2] for the uncertain system in the presence of unmodeled dynamics. Specifically, our study considers a quadcopter system (modeled dynamics) that carries a suspended load (unmodeled dynamics) under wind turbulance (disturbance) while trajectory tracking (see Figure 1). To elucidate the efficacy of this technique experimentally, we also compare the performance of the aforementioned model reference adaptive control architecture with its standard counterpart (see, for example, [1] and [Section 2, 2]).

Notation presented in this paper is as follows: $\mathbb{R}$ denotes the set of real numbers, $\mathbb{R}^n$ denotes the set of $n\times 1$ real column vectors, $\mathbb{R}^{n\times m}$ denotes the set of $n\times m$ real matrices, $\mathbb{R}_+$ (respectively, $\overline{\mathbb{R}}_+$) denotes the set of positive (respectively, nonnegative) real numbers, $\mathbb{R}_+^{n\times n}$ (respectively, $\overline{\mathbb{R}}_+^{n\times n}$) denotes the set of $n\times n$ positive-definite (respectively, nonnegative-definite) real matrices, $\mathbb{S}^{n\times n}$ denotes the set of $n\times n$ symmetric real matrices, $\mathbb{D}^{n\times n}$ denotes the set of $n\times n$ real matrices with diagonal scalar entries, and "$\triangleq$" denotes the equality by definition.

The rest of the paper is organized as follows. In Section II, we overview the theory of Model Reference Adaptive Control augmented with the adaptive robustifying term. Detailed experimental setup and experimental

results are presented in Section III. Finally, concluding remarks are given in Section IV.

## II Model Reference Adaptive Control in the Presence of Unmodeled Dynamics: Overview of [Section 3, 2]

This section provides a concise overview of [Section 3, 2]. In particular, consider the uncertain dynamical system with unmodeled dynamics given by

$$\dot{x}(t) = Ax(t) + B\Lambda u(t) + B\delta(x(t)) + Bp(t), \quad x(0) = x_0, \tag{1}$$

$$\dot{q}(t) = Fq(t) + G_1\Lambda u(t) + G_2 x(t), \quad q(0) = q_0, \tag{2}$$

$$p(t) = Hq(t), \tag{3}$$

where $x(t) \in \mathbb{R}^n$ is the measurable state vector, $u(t) \in \mathbb{R}^m$ is the control input, $q(t) \in \mathbb{R}^p$ and $p(t) \in \mathbb{R}^m$, respectively are the unmodeled dynamics state and output vectors, $A \in \mathbb{R}^{n\times n}$ is a known system matrix, $B \in \mathbb{R}^{n\times m}$ is a known input matrix (the pair $(A, B)$ is controllable), $\Lambda \in \mathbb{R}_+^{m\times m} \cap \mathbb{D}^{m\times m}$ is an unknown control effectiveness matrix (that naturally satisfies $\lambda_L \leq \|\Lambda\|_2 \leq \lambda_U$ with $\lambda_L \in \mathbb{R}_+$ and $\lambda_U \in \mathbb{R}_+$), $\delta(x) : \mathbb{R}^n \to R^m$ is a system uncertainty that can be parametrized as $\delta(x) = W_0^{\mathrm{T}}\sigma_0(x)$ with $W_0 \in \mathbb{R}^{s\times m}$ being an unknown weight matrix and $\sigma_0 \in \mathbb{R}^n \to \mathbb{R}^s$ being a known basis function, and $F \in \mathbb{R}^{p\times p}, G_1 \in \mathbb{R}^{p\times m}, G_2 \in \mathbb{R}^{p\times n}$, and $H \in \mathbb{R}^{m\times p}$ are matrices associated with unmodeled dynamics with $F$ being Hurwitz.

Next, consider the reference model, which captures a desired closed-loop system performance, given by

$$\dot{x}_{\mathrm{r}}(t) = A_{\mathrm{r}}x_{\mathrm{r}}(t) + B_{\mathrm{r}}c(t), \quad x_{\mathrm{r}}(0) = x_{r0}, \tag{4}$$

where $x_{\mathrm{r}}(t) \in \mathbb{R}^n$ is the reference state vector, $c(t) \in \mathbb{R}^m$ is a given uniformly continuous bounded command, $A_{\mathrm{r}} \in \mathbb{R}^{n\times n}$ is the Hurwitz reference system matrix, and $B_{\mathrm{r}} \in \mathbb{R}^{n\times m}$ is the command input matrix. Note that since $A_{\mathrm{r}}$ is Hurwitz, there exist $P \in \mathbb{R}_+^{n\times n} \cap \mathbb{S}^{n\times n}$ such that $0 = A_{\mathrm{r}}^{\mathrm{T}}P + PA_{\mathrm{r}} + I$ holds.

In standard model reference adaptive control algorithms predicated on the projection operator (see, for example, [1] and [Section 2, 2]), the feedback control law takes the form

$$u(t) = -K_1x(t) + K_2c(t) - \hat{W}^{\mathrm{T}}(t)\sigma(\cdot). \tag{5}$$

where $K_1 \in \mathbb{R}^{m\times n}$ and $K_2 \in \mathbb{R}^{m\times m}$ are the feedback and feedforward gains respectively such that $A_{\mathrm{r}} \triangleq A - BK_1$ and $B_{\mathrm{r}} \triangleq BK_2$. Moreover, in (5), $\hat{W}(t) \in \mathbb{R}^{s\times m}$ is an estimate of the unknown weight $W_0$ satisfying the weight update law given by

$$\dot{\hat{W}}(t) = \gamma \operatorname{Proj}_{\mathrm{m}}\left[\hat{W}(t), \sigma(\cdot)e^{\mathrm{T}}(t)PB\right], \quad \hat{W}(0) = \hat{W}_0, \tag{6}$$

with $\gamma \in \mathbb{R}_+$ being the learning rate. On the other hand, for the model reference adaptive control algorithm in [Section 3, 2], the feedback control law takes the form

$$u(t) = -K_1x(t) + K_2c(t) - \hat{W}^{\mathrm{T}}(t)\sigma(\cdot) - \hat{\mu}(t)B^{\mathrm{T}}Pe(t), \tag{7}$$

where $\hat{\mu}(t)$, adaptive robustifying term, satisfies

$$\dot{\hat{\mu}}(t) = \mu_0 \operatorname{Proj}\left(\hat{\mu}(t), \left\|B^{\mathrm{T}}Pe(t)\right\|_2^2 - \sigma_\mu\hat{\mu}(t)\right), \quad \hat{\mu}(0) = \hat{\mu}_0, \quad \hat{\mu}_0 \in \overline{R}_+, \tag{8}$$

with $\mu_0 \in \mathbb{R}_+$ and $\sigma_\mu \in \mathbb{R}_+$ being design parameters.

We refer to [Section 2, 2] (and [1]) for the sufficient stability condition resulting from (5) and [Section 3, 2] for the sufficient stability condition resulting from (7). In what follows, we present the experimental setup considered in this paper.

# III Experiments

## A Experimental Setup

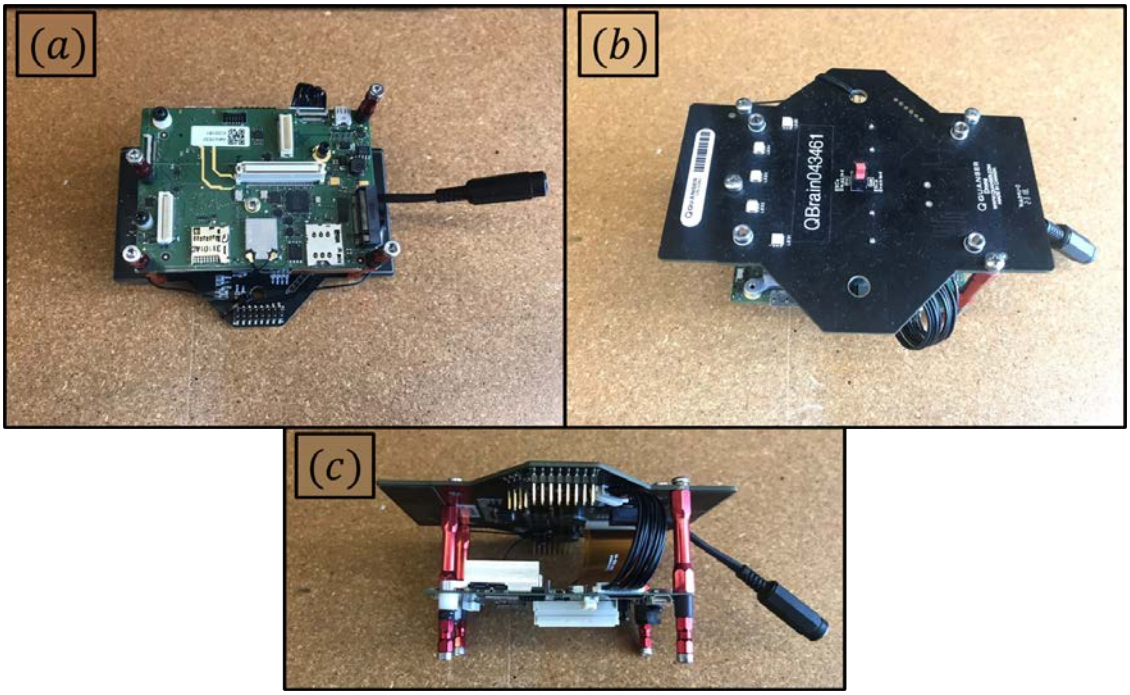


Figure 2: Main computing board used in the quadrotor-QBrain; (a) Top view, (b) bottom view, and (c) side view.

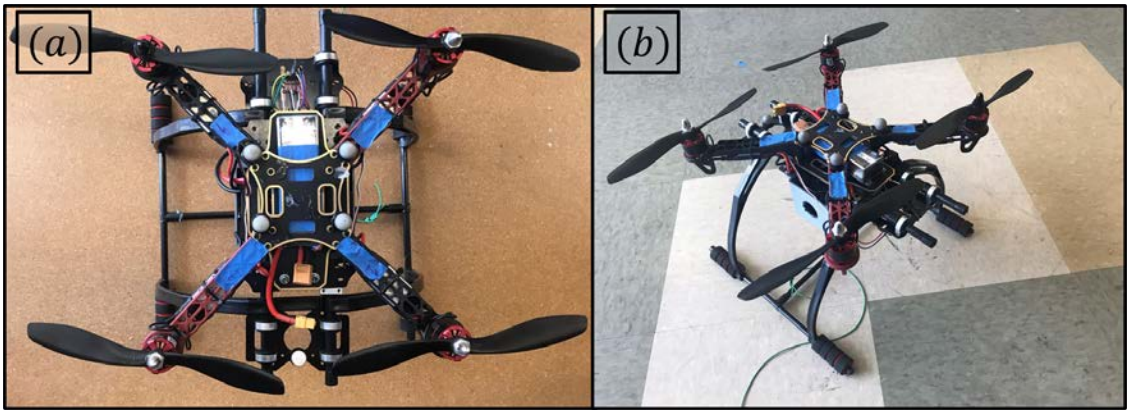


Figure 3: Custom built quadcopter: (a) Top view and (b) isometric view.

This section presents details with regard to a custom built quadcopter system (modeled dynamics) carrying a load (unmodeled dynamics). In particular, readily available off-the-shelf components are used to build the quadcopter such as motors, electronic speed controllers, propellers, and a frame. The main processing unit is QBrain (see [12]). The QBrain is equipped with 6-DOF 16-bit 3-axial accelerometer and gyroscope, 3-axis geomagnetic sensor, and 24-bit pressure and temperature sensor. Moreover, the unit has an IEEE 802.11 b,g,n,ac - Intel Dual Band Wireless - AC 8620 2x2 MIMO chip. Matlab/Simulink software is used to design the autopilot of the quadrotor and at the same time implement the different feedback control strategies (see the previous section).

The QBrain is connected to a wireless router that is connected to a PC that runs Matlab/Simulink model in external mode, a function which QBrain supports. Figure 2 shows the QBrain computing unit and Figure 3 shows one of the custom built quadrotors that we used in the experiments.

As stated above, the scenario of this experimental study is transportation of an object that is connected to the quadrotor with a rope through a trajectory, see Figure 1. This allows us to compare the performance of [Section 3, 2] with its standard counterpart (see, for example, [1] and [Section 2, 2]). In addition, we use a fan to introduce external disturbance.

## B Autopilot

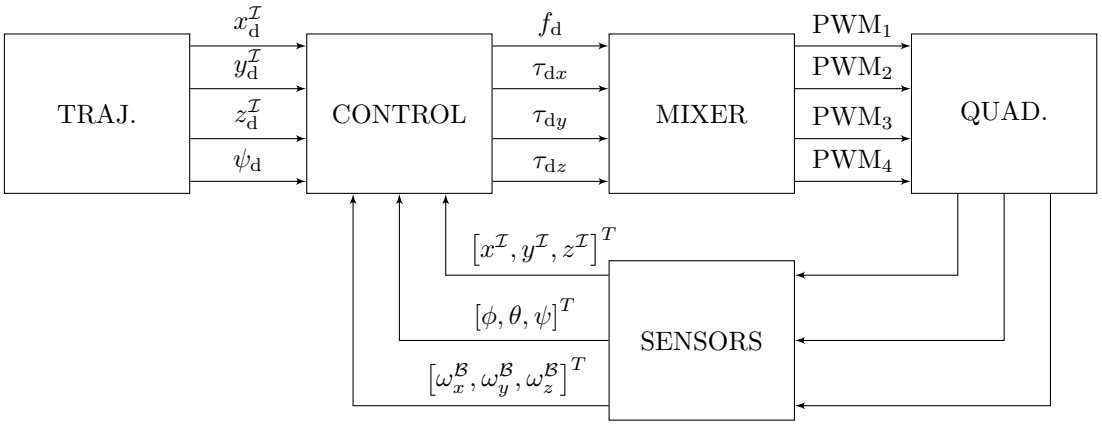


Figure 4: Autopilot.

The block diagram in Figure 4 shows the general structure of the autopilot we programmed for the experiments. The trajectory block generates a desired trajectory for the quadcopter to track.

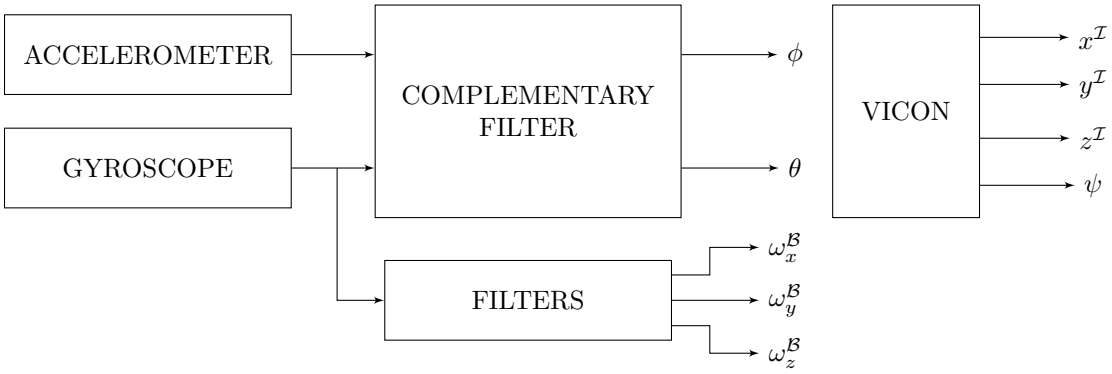


Figure 5: Sensors block diagram.

The autopilot algorithm demands for the measurements of the quadcopter states. To this end, the gyroscope provides the angular velocities $\omega_x^{\mathcal{B}}$, $\omega_y^{\mathcal{B}}$, and $\omega_z^{\mathcal{B}}$ with respect to body fixed frame. A complementary filter, a sensor fusion technique, estimates the two of the euler angles which are pitch $\theta$ and roll $\phi$ by processing the accelerometer and the gyroscope data. A VICON motion capture system provides real-time data for the position of the quadcopter in 3D space $x^{\mathcal{I}}$, $y^{\mathcal{I}}$, and $z^{\mathcal{I}}$ with respect to the inertial frame, and the last euler angle which is yaw $\psi$. Figure 5 shows the available sensors and data with a block diagram. Nominal control and MRAC parameters are available in Table 1.

Figure 6 shows the control structure. There are four seperate control laws. Three of them for the position tracking in $x^{\mathcal{I}}$, $y^{\mathcal{I}}$, and $z^{\mathcal{I}}$, and the last one is for the tracking in $\psi$. The control law for $x^{\mathcal{I}}$ and $y^{\mathcal{I}}$ consist of

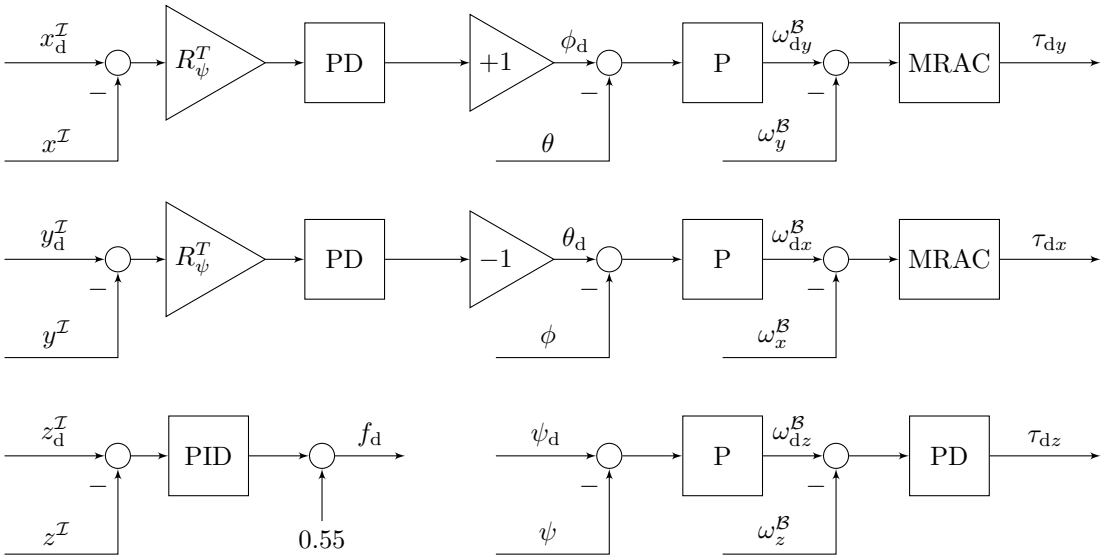


Figure 6: The control structure

Table 1: Control parameters

| **Position PID** | | | | **Euler Ang. P** | | **Ang. Vel. PD** | | | **Angular Velocity MRAC** | | | | |
|---|---|---|---|---|---|---|---|---|---|---|---|---|---|
| **Axis** | **P** | **I** | **D** | **Angle** | **P** | **Axis** | **P** | **D** | **Axis** | $\gamma$ | $A_r$ | $\sigma_0$ | $\sigma_\mu$ |
| $x$ | 0.6 | 0 | 0.3 | $\phi$ | 7 | $x$ | 0.15 | 0.003 | $x$ | 0.3 | $-64$ | 1.1 | 0.4 |
| $y$ | 0.6 | 0 | 0.3 | $\theta$ | 7 | $y$ | 0.15 | 0.003 | $y$ | 0.3 | $-64$ | 1.1 | 0.4 |
| $z$ | 0.6 | 0.1 | 0.3 | $\psi$ | 5 | $z$ | 0.2 | 0 | | | | | |

three nested loops. The outer loops are PD controllers for the positions $x^{\mathcal{I}}$ and $y^{\mathcal{I}}$, the intermediate loops are P controllers for the Euler angles $\phi$ and $\theta$. The most inner loop control the angular velocities $\omega_y^{\mathcal{B}}$ and $\omega_x^{\mathcal{B}}$ with three different structures for three different scenarios:

(C1) PD controller as a *nominal controller*,

(C2) *Model reference adaptive controller* (MRAC),

(C3) *MRAC augmented with the adaptive robustifying term*

The control law for the altitude $z^{\mathcal{I}}$ is a PID controller. The control law for the yaw contains two nested loops where the outer loop controls $\psi$ and the inner loop controls $\omega_z^{\mathcal{B}}$. The output of the control block is the desired thrust $f_{\mathrm{d}}$, and the desired torques $\tau_{\mathrm{d}x}$, $\tau_{\mathrm{d}y}$, and $\tau_{\mathrm{d}z}$.

A mixer function converts $f_{\mathrm{d}}$, $\tau_{\mathrm{d}x}$, $\tau_{\mathrm{d}y}$, and $\tau_{\mathrm{d}z}$ to PWM signals which is shown in Figure 7. PWM signals are fed to the electronic speed controllers to set the rotational speeds of BLDC motors to generate the desired thrust and torques.

## C Experimental Results

In this section, we present the experimental results of the quadcopter (modeled dynamics) carrying a suspended load (unmodeled dynamics) while tracking a trajectory. The load mass is 300 grams. Furthermore, a large fan generates wind in the direction of $y-$axis of the inertial frame to disturb the quadcopter system during the experiments. To excite the unmodeled dynamics as much as possible, the desired trajectory is a square with sharp

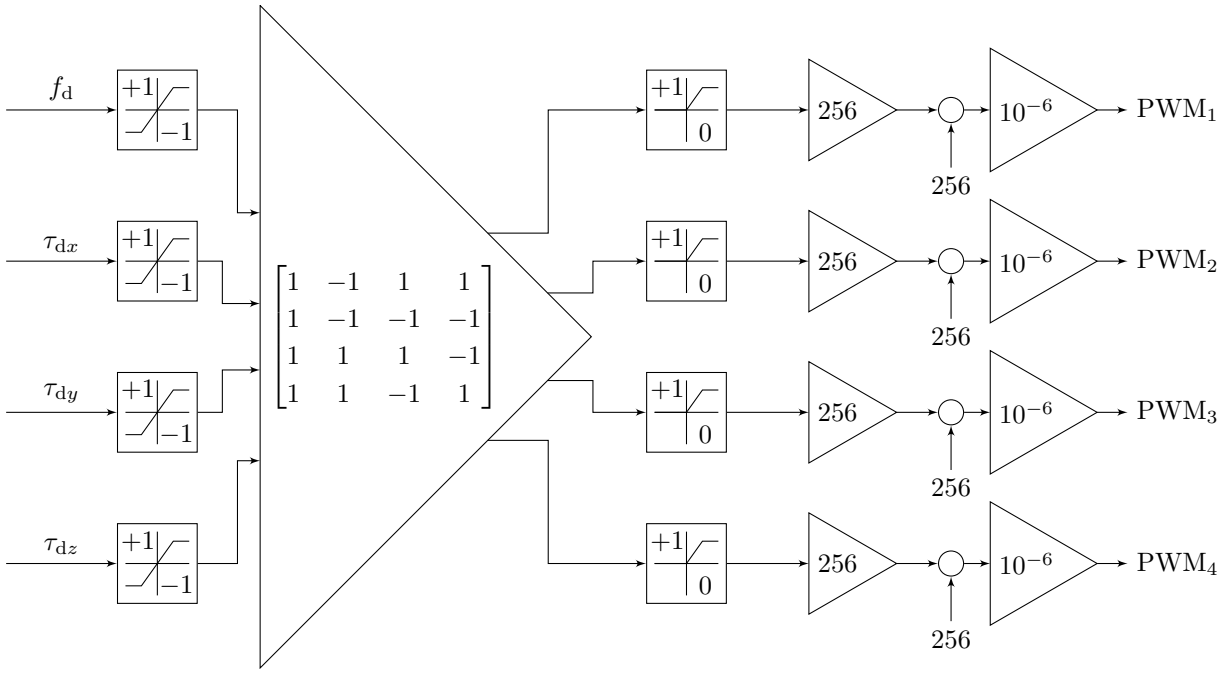


Figure 7: Mixer functions.

edges in $xy-$plane and constant in altitude and yaw angle. Each edge of the square is one meter, and the altitude is set to one meter. We compare the performance of three different control structures described in Section B.

We present the experimental results for control strategy (C1), (C2), and (C3) in Figure 8, Figure 9, and Figure 10 respectively. Since the quadcopter stays a constant height, we only plot the quadcopter's position $x(t)$ and $y(t)$, quadcopter's pitch and roll angles with respect to time and their rates. In addition, we present a $xy$ plot of the quadcopter's position for visualization. Immediate observation from figures is that (C2) and (C3) have better tracking performance in $x$ and $y$ than (C1). There is a significant tracking error in the $y-$axis with (C1) due to the wind generated through $y-$axis whereas (C2) and (C3) efficiently remove the effect of this constant disturbance due to the wind.

Observe that (C2) improves the tracking error significantly compared to (C1), however, it introduces oscilations in pitch and roll rates, compare for example Figure 8 and Figure 9. Finally, with (C3) oscilations in pitch and roll rates are removed while having similar tracking performace as (C2), compare for example Figure 9 to Figure 10. Normalized errors in $x(t)$, $y(t)$, Pitch ($\theta(t)$), Roll ($\phi(t)$), Pitch rate ($\dot{\theta}(t)$), and Roll rate ($\dot{\phi}(t)$) are summarized in Table 2.

## IV Conclusion

In this paper, we experimentally elucidated the efficacy of the Model Reference Adaptive Controller augmented with a robustifying adaptive term to nullify the effect of unmodeled dynamics (for example, quadcopter carrying a load in the presence of external disturbances). Using our custom built quadcopter based on Quanser's Qbrain autopilot, We have experimentally tested three different controllers: the nominal controller, the model reference adaptive controller, and the model reference adaptive controller augmented with the robustifying adaptive term. Experimental results showed that the last control approach strategy sufficiently eliminated the disturbances while decreasing tracking error.

Table 2: Summary of normalized errors in $x(t)$, $y(t)$, Pitch ($\theta(t)$), Roll ($\phi(t)$), Pitch rate ($\omega_y^{\mathcal{B}}(t)$), and Roll rate ($\omega_x^{\mathcal{B}}(t)$).

| **Normalized Error** | Controller Type | | |
|---|---|---|---|
| | **(C1)** | **(C2)** | **(C3)** |
| $\left\|x^{\mathcal{I}}(t) - x_{\mathrm{d}}^{\mathcal{I}}(t)\right\|_2$ | 0.48700 | 0.35491 | 0.29275 |
| $\left\|y^{\mathcal{I}}(t) - y_{\mathrm{d}}^{\mathcal{I}}(t)\right\|_2$ | 0.19595 | 0.39234 | 0.24063 |
| $\left\|\theta(t) - \theta_{\mathrm{d}}(t)\right\|_2$ | 0.09613 | 0.21143 | 0.08511 |
| $\left\|\phi(t) - \phi_{\mathrm{d}}(t)\right\|_2$ | 0.10580 | 0.13553 | 0.09425 |
| $\left\|\omega_x^{\mathcal{B}}(t) - \omega_{\mathrm{d}x}^{\mathcal{B}}(t)\right\|_2$ | 0.48474 | 1.69366 | 0.41253 |
| $\left\|\omega_y^{\mathcal{B}}(t) - \omega_{\mathrm{d}y}^{\mathcal{B}}(t)\right\|_2$ | 0.49332 | 1.33869 | 0.46837 |

## Acknowledgement

We would like to thank Esra Koru for taking and editing the photo in Figure 1.

## References

[1]M. Matsutani, A. M. Annaswamy, T. E. Gibson, and E. Lavretsky, "Trustable autonomous systems using adaptive control," in *2011 50th IEEE Conference on Decision and Control and European Control Conference*. IEEE, 2011, pp. 6760–6764.

[2]K. M. Dogan, B. C. Gruenwald, T. Yucelen, and J. A. Muse, "Relaxing the stability limit of adaptive control systems in the presence of unmodelled dynamics," *International Journal of Control*, vol. 91, no. 8, pp. 1774–1784, 2018.

[3]M. Matsutani, A. Annaswamy, and E. Lavretsky, "Guaranteed delay margins for adaptive control of scalar plants," in *2012 IEEE 51st IEEE Conference on Decision and Control (CDC)*. IEEE, 2012, pp. 7297–7302.

[4]M. Matsutani, "Robust adaptive flight control systems in the presence of time delay," Ph.D. dissertation, Massachusetts Institute of Technology, 2013.

[5]H. S. Hussain, M. M. Matsutani, A. M. Annaswamy, and E. Lavretsky, "Adaptive control of scalar plants in the presence of unmodeled dynamics," *IFAC Proceedings Volumes*, vol. 46, no. 11, pp. 540–545, 2013.

[6]H. S. Hussain, M. Matsutani, A. M. Annaswamy, and E. Lavretsky, "Robust adaptive control in the presence of unmodeled dynamics: A counter to rohrs's counterexample," in *AIAA Guidance, Navigation, and Control (GNC) Conference*, 2013, p. 4753.

[7]K. M. Dogan, T. Yucelen, B. C. Gruenwald, and J. A. Muse, "On model reference adaptive control for uncertain dynamical systems with unmodeled dynamics," in *2016 IEEE 55th Conference on Decision and Control (CDC)*. IEEE, 2016, pp. 377–382.

[8]K. M. Dogan, B. C. Gruenwald, T. Yucelen, and J. A. Muse, "On the stability of adaptive control systems in the presence of control and state dependent unmodeled dynamics," in *AIAA Guidance, Navigation, and Control Conference*, 2017, p. 1717.

[9]K. M. Dogan, T. Yucelen, B. C. Gruenwald, and J. A. Muse, "Stability conditions for adaptive control of uncertain dynamical systems with actuator and unmodeled dynamics," in *2018 Annual American Control Conference (ACC)*. IEEE, 2018, pp. 5442–5447.

[10]K. M. Dogan, B. C. Gruenwald, T. Yucelen, and J. A. Muse, "A generalization of fundamental stability limits of model reference adaptive controllers in the presence of a class of nonlinear unmodeled dynamics," in *2018 AIAA Guidance, Navigation, and Control Conference*, 2018, p. 1309.

[11]K. M. Dogan, T. Yucelen, E. Yildirim, and J. A. Muse, "Experimental results of a model reference adaptive control law on an uncertain system with unmodeled dynamics," in *AIAA Scitech 2019 Forum*, 2019, p. 2336.

[12]Quanser. (1989) High-performance drone for indoor labs. [Online]. Available: https://www.quanser.com/products/qdrone/

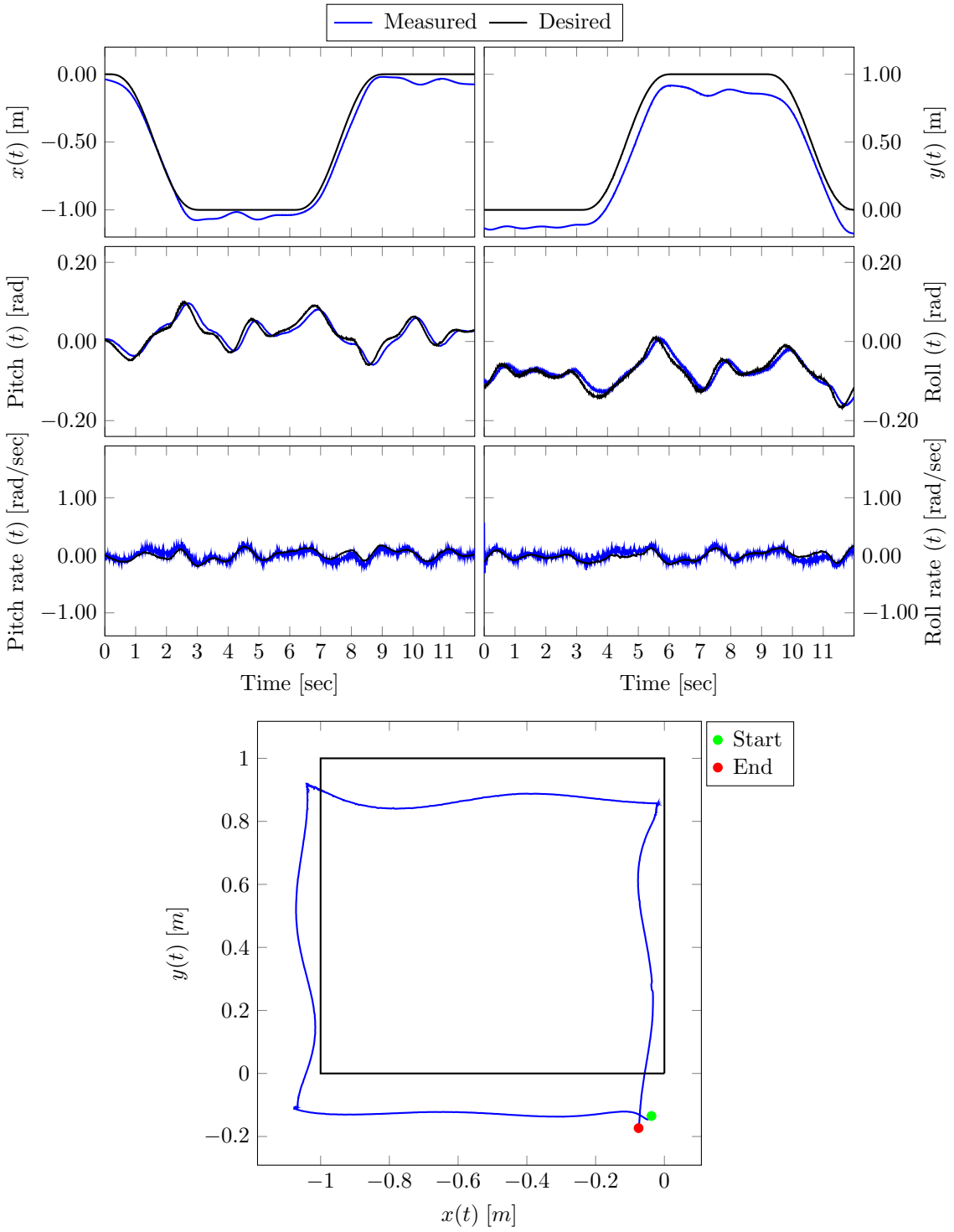


Figure 8: Experimental result using the nominal controller, (C1).

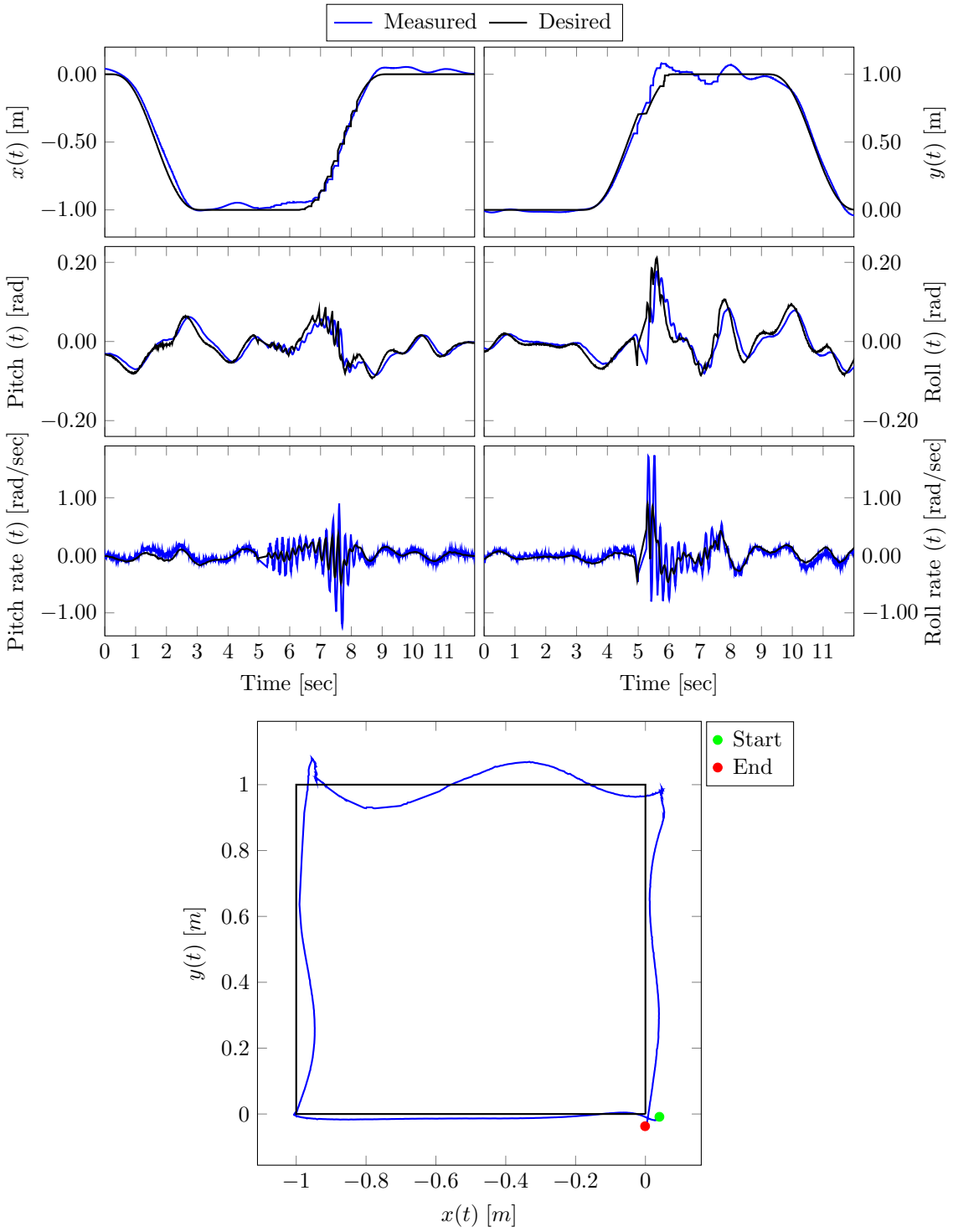


Figure 9: Experimental result using the Model Reference Adaptive Controller, (C2).

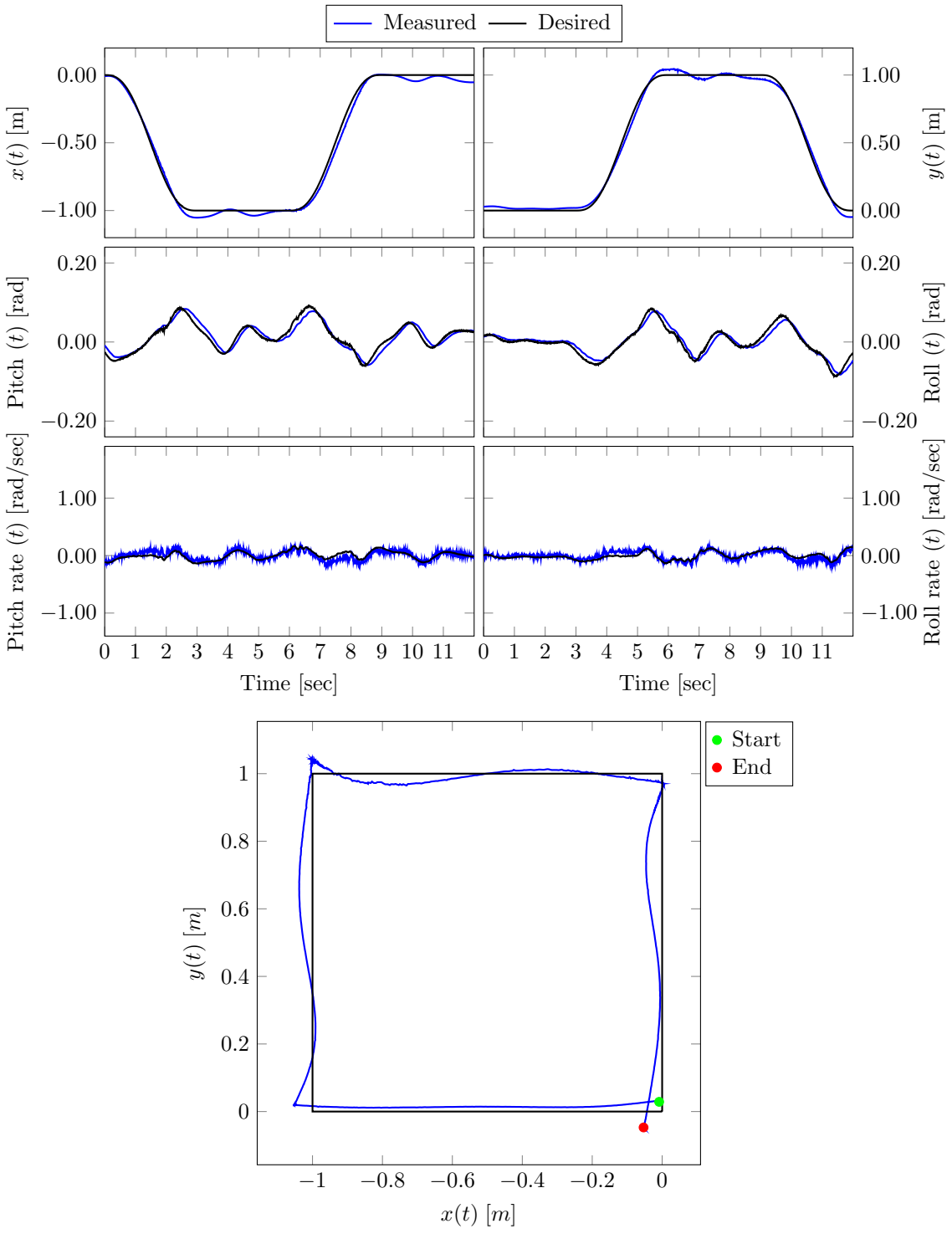


Figure 10: Experimental result using the Augmented Model Reference Adaptive Controller with adaptive robustifying term, (C3).